Contrib. Mineral. Petrol. 67, 139–149 (1978)

Contributions to Mineralogy and Petrology

Skeletal Crystallization and Residual Glass Compositions in a Cellular Alkalic Pyroxenite Nodule From Oldoinyo Lengai

Implications for Evolution of the Alkalic Carbonatite Lavas

Colin H. Donaldson[1] and J. Barry Dawson[2]*

[1] Department of Geology, University of St. Andrews, St. Andrews, Fife KY16 9ST, Scotland
[2] Department of Geology, University of St. Andrews, St. Andrews, Scotland

Abstract. The alkalic pyroxenite nodule consists of megacrysts of diopside, apatite, perovskite and titanomagnetite in a groundmass consisting of diopside, apatite, titanomagnetite, nepheline, melilite, garnet and vishnevite crystals of various shapes, including previously undescribed skeletal and dendritic shapes, together with vesicles and residual glass. The residual glass is poor in SiO_2 (38–40 wt%), and extraordinarily rich in Na_2O (12.8–15 wt%), SO_3 (1–1.5 wt%), and Cl (0.25–0.7 wt%), as a result of rapid, non-equilibrium crystallization of groundmass phases from a CO_2-rich nephelinite melt.

The Oldoinyo Lengai alkalic carbonatite lavas do not represent extreme products of the fractional crystallization of pyroxene, wollastonite, nepheline and alkali feldspar from the carbonated nephelinite melt. The most likely connection between the carbonatite and silicate magma types is one of liquid immiscibility, probably involving phonolite melt.

Introduction

The active volcano Oldoinyo Lengai, Tanzania, consists mainly of nephelinitic and phonolitic pyroclasts (Dawson, 1962a) and is famous for its extrusions of alkalic carbonatite lava and ashes (Dawson, 1962b; Dawson et al., 1968). The pyroclasts contain nodules of a wide variety of rocks, including ijolite, nepheline-syenite, fenite, wollastonite, glimmerite, biotite-pyroxenite, pyroxenite and sovite, that indicate the presence of a plutonic/hypabössal complex beneath the volcano, composed of carbonatite and alkalic silicate rocks. The ijolite is particularly interesting as it is probably of magmatic origin (Bell et al., 1973).

In this paper we describe the petrology of a cellular alkalic pyroxenite nodule consisting of randomly oriented megacrysts cemented by subordinate amounts of intergranular glass containing a variety of fine-grained minerals with euhedral, skeletal and dendritic shapes. The study provides clues to the nature of the magma parental to the silicate rocks, to the phases fractionating from the magma and to the genetic relationship between the silicate and carbonate magmas erupted by the volcano.

Sample Description

The cellular alkalic pyroxenite block (BD878) was collected on the southern lower flanks of the volcano from the prehistoric yellow phonolitic pyroclasts that form the bulk of the volcano. Similar cellular pyroxenite and ijolite blocks were found in ejectamenta during the 1960 survey of Oldoinyo Lengai (Dawson, 1962a) and again during the 1966 eruption (Dawson et al., 1968). Hence the implications of this study are believed to be generally relevant to possible petrogenetic processes throughout the eruption history.

Table 1. Modal composition of alkalic pyroxenite nodule (volume percent)[a]

Megacrysts	Pyroxene	66.8
	Apatite	1.2
	Perovskite	3.9
	Titanomagnetite	<0.1
Groundmass	Glass	7.5
	Garnet	0.1
	Titanomagnetite	0.2
	Apatite	2.6
	Nepheline	4.4
	Pyroxene	1.8
	Melilite	0.6
	Vishnevite	3.3
	Vesicles	7.6
	Calcite	<0.1

[a] Determined by point counting (9424 counts)

* Present address: Dept. of Geology, University of Sheffield, Sheffield S1 3JD

0010-7999/78/0067/0139/$02.20

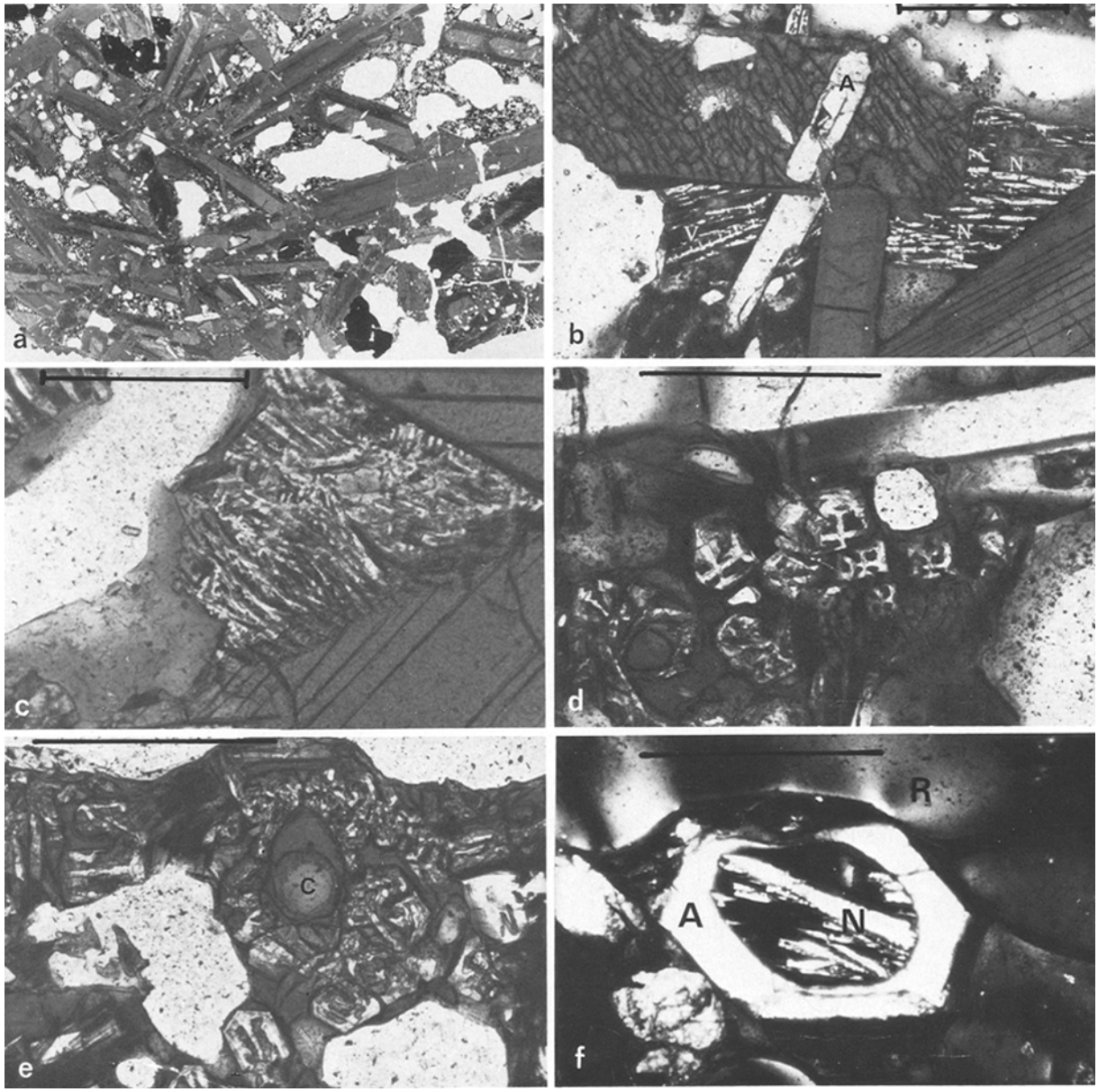

Fig. 1. **a** Part of a thin section of BD878 showing cellular structure due to gas cavities between megacrysts of zoned pyroxene and opaque phases. Field width = 35 mm. **b** Zoned pyroxene (one partially enclosing apatite-A), and interstitial glass containing chain vishnevite (*V*) (cut parallel to **c** axis) and parallel-growth nepheline (*N*). Scale bar = 1 mm; plane-polarised light (p.p.l.). **c** Single crystal of feather nepheline in residual glass between two pyroxene crystals. Scale bar = 0.5 mm; p.p.l. **d** Skeletal vishnevites, cut normal to *c* axis, showing Malteose Cross-shaped sections. Scale bar = 0.5 mm; p.p.l. **e** Hopper/vermicular vishnevite within residual glass, surrounding gas cavities, one of which (*C*) has not been breached during sectioning. Scale bar = 0.5 mm; p.p.l. **f** Hollow apatite (*A*) containing isotropic glass from which nepheline (*N*) has crystallised. Part of field is occupied by non-isotropic resin (*R*); crossed polarisers; scale bar = 0.5 mm

Prior to sectioning the oval block measured approximately $12 \times 10 \times 8$ cm; the surface is uneven with many cavities penetrating from the surface into the interior of the block.

In thin section, the rock consists mainly of megacrysts of pyroxene with lesser amounts of titanomagnetite, perovskite and apatite megacrysts, bonded by interstitial glass within which are minor amounts of crystalline phases (Table 1). Since the rock contains > 70 vol% mafic minerals it is a *melteigite*; however we prefer to use the simpler, more descriptive term *alkalic pyroxenite*. A striking feature is the presence of numerous round or irregular-shaped voids or vesicles in between the megacrysts (Fig. 1a). The ratio of void to interstitial glass is variable (the abundances of these two components in Table 1 are effectively averages). In some parts of the specimen the glass (with groundmass phases) fills all the inter-megacryst space, whereas in others it forms only a thin veneer on the megacrysts, and a concave boundary to the void.

The pyroxene megacrysts are platy (up to 30 mm across × 4 mm thick), euhedral, and zoned from brown-green cores to darker-green rims; they partially enclose elongate subhedral apatite crystals (up to 1.5 cm long) (Fig. 1b) and also anhedral crystals of titanomagnetite and faintly birefringent perovskite, both

up to 5 mm in size. The interstitial glass is mainly olive-green in colour and is the matrix to smaller crystals of bright-green and deep-green pyroxenes, melilite, brown garnet, apatite, nepheline, vishnevite (sulphur-rich cancrinite) and calcite. Garnet is rare and forms <0.01 mm wide euhedral grains within euhedral melilite grains which vary in size up to 1 mm. Whereas the groundmass pyroxene, titanomagnetite and garnet are euhedral, the apatite, melilite, nepheline and vishnevite adopt a variety of morphologies. Most apatite is subhedral but a few crystals have hopper morphology. Some melilites are euhedral and rectangular in section, whereas others exhibit hopper and parallel-growth morphologies. (For examples of these types of morphology see Donaldson, 1976.) The nephelines show euhedral, hopper and linked parallel-growth morphologies and also occur as feather dendrites (Fig. 1 b and c). Vishnevite forms both chain crystals and hopper/vermicular crystals (Fig. 1 b, d and e); in sections cut normal to the *c* axis the chain morphology is that of a Maltese Cross (Fig. 1 d). Furthermore, vishnevite crystals are usually the phase closest to glass/vesicle boundaries and sometimes are arranged concentric to the vesicles (Fig. 1 e). Scarce calcite (<0.1 vol%) has crystallised in small (0.3 mm) ovoid patches in the groundmass, some of which partially enclose feather dendrites of nepheline.

The crystal size and textural relations suggest (a) a period of slow crystallization of the megacrysts, during which the order of crystallization was apatite – titanomagnetite and perovskite – pyroxene; followed by (b) a stage in which groundmass pyroxene, apatite, garnet, titanomagnetite, euhedral nepheline and euhedral melilite grew from a liquid with which some of them were not fully equilibrating during cooling (as witnessed by the zoning); then (c) rapid cooling causing growth of the skeletal melilite, nepheline and vishnevite, probably with the vishnevite and calcite being the final phases to crystallize.

To the best of our knowledge, this is the first report of skeletal melilite, nepheline and vishnevite in rocks. Hopper apatite has been grown in the laboratory under rapid crystallization conditions (Wyllie et al., 1962) and skeletal and dendritic nepheline crystals, similar to those in Fig. 1 b and c have been grown from nephelinite melts cooled at >2°/h (Lofgren, unpublished data).

Bulk Composition

A bulk analysis (Table 2) shows the rock to be low in SiO_2 and Al_2O_3 but high in TiO_2, iron (both FeO and Fe_2O_3), CaO, MgO, F, and Cl. The composition obviously reflects the high pyroxene content of the rock, but the low SiO_2 content reflects both the presence of oxide minerals and the undersaturated nature of the interstitial glass and its crystalline phases. The Na_2O/K_2O ratio of 4:1 is a characteristic of many of the silicate lavas from Oldoinyo Lengai and also of the alkalic carbonatite lavas. The low H_2O^+ and high CO_2 contents (despite the trivial amount of carbonate present) are taken as evidence that the ratio of CO_2/H_2O in the magma was high (cf. Heiken, 1974). The Fe^{3+}/Fe^{2+} ratio exceeds 1; however, in view of the structural effect of melts (caused by alkalis) on $Fe^{3+}/\Sigma Fe$ ratio (Virgo and Mysen, 1977), this should not be assumed to reflect highly oxidizing conditions.

Phase Compositions

Energy-dispersive analyses of glass and selected crystals were obtained with the Manchester University electron microprobe, using a sample current of 4 nA and counting for 100 seconds on each 2 micron-wide spot. Analyses were corrected for deadtime, fluorescence, absorption and atomic number using a commercial computer program (Link Systems Inc.). At the low sample currents used alkali mobility was not a problem. The analyses in Tables 3–8 represent the widest range of compositions found.

Table 2. Bulk analysis of alkalic pyroxenite nodule

SiO_2	32.54
TiO_2	5.78
Al_2O_3	5.64
Fe_2O_3	13.10
FeO	10.44
MnO	0.32
MgO	7.18
CaO	18.36
Na_2O	2.96
K_2O	0.75
P_2O_5	1.94
H_2O^+	0.37
H_2O^-	0.27
CO_2	0.46
Total	100.11
$Na_2O:K_2O$	3.95
$CO_2:(CO_2+H_2O^+)$ molar	0.34
Analyst: J.R. Baldwin	
F 1,204 ppm	
Cl 730 ppm	
Analyst: R. Fuge	

1. Perovskite and Titanomagnetite (Table 3). The perovskite megacrysts are Fe-poor but contain >1% Na_2O. The weak birefringence is attributable to lattice distortion caused by solid solution of *dysanalyte* molecule (Deer et al., 1962). The titanomagnetite megacrysts differ from the groundmass crystals in containing more Mg, Al, and Ti and also in having a lower Fe^{3+}/Fe^{2+} ratio. The high MnO content (>0.7%) of both megacrysts and groundmass crystals is noteworthy.

2. Apatite and Calcite. All the apatite crystals, whether megacryst or groundmass or of differing morphology, have simple compositions consisting only of Ca and P; no Cl or F has been detected and analyses totals (shortfall of ~0.2–0.4%) do not suggest significant quantities of CO_2 or H_2O. The calcite has an equally simple composition with only Ca being detected.

3. Pyroxenes (Table 4). The pyroxenes are all Ca-rich, lying close to the diopside-hedenbergite join of the pyroxene quadrilateral; overall they contain 11–20 mol% of components other than $CaSiO_3$ and $FeSiO_3$, the most abundant of which are acmite (3.8–12.8 mol%), $CaTiAl_2O_6$ molecule (1.1–7.3%) and Ca-Tschermak's molecule (0–3.5 mol%). Considering the low Na_2O and hence acmite content of all the crystals (Table 4), the intense green colour of the megacrysts is most unusual. The megacryst rims contain lower TiO_2 (possibly due to earlier depletion by precipitation of perovskite and titanomagnetite), Al_2O_3, Na_2O and Al^{IV} and also have higher Fe^{2+}/Fe^{3+} and Al^{VI}/Al^{IV} ratios. Some groundmass pyroxenes are sector-zoned, and the compositions of the margins of [010] sectors resemble megacryst cores whereas margins of [001] sectors resemble megacryst rims (Table 4, Columns 3 and 4). The deep-green groundmass crystals have similar composition to the megacrysts whereas the bright-green ones are

Table 3. Perovskite and titanomagnetite analyses

	1	2	3
	Perovskite	Titanomagnetite	
	megacryst	megacryst	groundmass
MgO	0.00	2.66	1.75
Al_2O_3	0.00	1.90	0.52
FeO	0.97[a]	38.12[c]	34.77[c]
Fe_2O_3	–	43.72	52.22
MnO	0.00	0.71	0.77
TiO_2	54.48	12.55	8.23
CaO	35.38	0.00	0.00
Na_2O	1.11	0.00	0.00
	92.83[b]	99.66	98.26
Structure	0=3	0=4	0=4
Mg	–[d]	0.147	0.099
Al	–	0.083	0.023
Fe^{2+}	0.019	1.180	1.112
Fe^{3+}	–	1.218	1.503
Mn	–	0.022	0.025
Ti	0.968	0.314	0.237
Ca	0.904	–	–
Na	0.050	–	–

[a] All iron as FeO
[b] Nb, Ta, and Ce present, but not analysed
[c] Calculated according to method of Anderson (1968)
[d] Calculated assuming shortfall (7.17 wt%) is all CeO_2 ($\equiv$0.058 Ce^{2+} per formula unit)

Table 4. Pyroxene analyses[a]

	1	2	3	4	5
	Megacryst		Sector-zoned groundmass crystal		Euhedral, equant bright green groundmass crystal
	Core	Rim	Margin of [001] sector	Margin of [010] sector	
SiO_2	47.65	50.37	50.21	47.68	51.70
TiO_2	2.24	1.54	1.34	2.64	0.36
Al_2O_3	5.25	3.02	2.81	5.36	0.90
Fe_2O_3[b]	3.63	1.88	2.05	2.44	4.52
FeO	5.39	6.12	5.95	6.23	10.99
MnO	–[c]	–[c]	–[c]	–[c]	0.58
MgO	11.92	12.72	13.13	11.51	8.41
CaO	23.27	23.95	24.10	23.82	20.85
Na_2O	0.92	0.63	0.52	0.70	2.18
	99.90	100.04	99.90	100.13	100.72
Structural formula 0=6					
Si	1.801	1.887	1.890	1.797	1.991
Al	0.199	0.113	0.110	0.203	0.009
Al	0.035	0.020	0.015	0.035	0.032
Ti	0.064	0.043	0.038	0.075	0.011
Fe^{3+}	0.103	0.053	0.058	0.069	0.131
Fe^{2+}	0.170	0.192	0.187	0.196	0.354
Mn	0.000	0.000	0.000	0.000	0.019
Mg	0.671	0.710	0.737	0.647	0.483
Ca	0.942	0.961	0.972	0.962	0.860
Na	0.067	0.046	0.038	0.051	0.163
Mg	35.6	37.1	37.7	34.5	26.4
Fe ionic %	14.5	12.8	12.5	14.2	26.5
Ca	49.9	50.1	49.8	51.3	47.1

[a] Cr <0.09 wt%
[b] Calculated from the amount of Fe^{3+} needed to make the pyroxene molecules suggested by Kushiro (1962) and assuming stoichiometry and perfect analysis
[c] Mn <0.08 wt%

relatively enriched in both acmite and hedenbergite and, compared with the other pyroxenes, contain appreciably less TiO_2, Al_2O_3 and MgO (Table 4, Column 5); the associated enrichment in Na_2O, FeO, Fe_2O_3 is also accompanied by the presence of 0.58% MnO – an oxide below the levels of detection in the other pyroxenes. Crystallization of the megacryst pyroxenes was accompanied by apatite, perovskite and titanomagnetite, of which only the titanomagnetite contains MnO. It appears that partitioning of MnO initially favoured the melt until the residual liquid was highly fractionated.

The analyses in Table 4 closely resemble pyroxene compositions in two alkaline basalt intrusions – the Black Jack teschenite sill (Wilkinson, 1957) and the Red Hill teschenite (Hutton, 1943). Sector-zoned pyroxenes in melilite-bearing leucite nephelinite and bergalite from Nyiragongo (Sahama, 1976), a volcano with strong affinities with Oldoinyo Lengai, also are compositionally similar to the pyroxenes in Table 4.

4. Melilite (Table 5). Melilite crystals do not vary widely in composition, despite their variable morphology (compare slowly grown and rapidly grown crystals, Table 5, numbers 1, 4 and 5); there are small variations in Al and Si contents, *mg* ratio (Mg/(Mg+ΣFe)), Na/(Na+Ca) ratio, and the amount of Mn. Many of the euhedral crystals are step-zoned (Table 5, number 3), becoming more Fe- and Na-rich and more Ca-poor at their margins; Mg and Al decrease and increase respectively from the core to the middle zone but are then unchanged in the outer zone (Table 5).

Recalculation of the compositions into the molecules sodic melilite ($CaNaAlSi_2O_7$), akermanite, sodium-iron melilite (Ca Na Fe Si_2O_7), iron melilite (Ca_2 Fe Si_2O_7) and gehlenite (Table 5) indicates that the crystals contain 33–44 molec. % of sodic melilite and that none contains gehlenite molecule; this is in agreement with Sahama's (1967) observation on other volcanic, as opposed to contact metamorphic, melilites. However, unlike the volcanic melilites analysed by Sahama (1967) those from Oldoinyo Lengai show only slight Mg/Fe variation; the main variation is in the ratio of sodic melilite to akermanite which is well illustrated on an Al–Fe–Mg plot (Fig. 2). The Oldoinyo Lengai melilites have insufficient Al to satisfy all the Na present, hence the formation of Ca Na Fe Si_2O_7 molecule in the recalculations (Table 5). Sahama (1976) has found a small proportion of the melilites in a sample of bergalite from Nyiragongo to contain Ca Na Fe Si_2O_7 molecule and Le Bas (1977) reports similar melilites in a melilite-nephelinite lava from Kisingiri, Kenya; however, neither of these occurrences contains more than 2.6 molec. % Ca Na Fe Si_2O_7 (contrast Table 5).

Although the least sodic Oldoinyo Lengai crystals are comparable to those in the wide range of melilite-bearing rocks studied by El Goresy and Yoder (1974), our most sodic samples contain 10–11 molec. % more sodic melilite than the most sodic melilite-

Table 5. Melilite analyses

	1 Square crystal	2 Square crystal	3 Elongate step-zoned crystal			4 Skeleton	5 Parallel-growth
			Core	Middle	Rim		
SiO_2	43.29	44.08	43.82	44.10	43.82	44.13	43.41
Al_2O_3	6.19	8.53	7.44	8.28	7.96	6.79	6.85
FeO	6.60	5.65	6.04	5.93	6.75	6.05	6.90
MnO	0.26	<0.08	0.27	<0.08	0.21	0.23	<0.08
MgO	6.03	5.34	5.48	4.99	5.07	5.96	5.40
CaO	32.18	31.93	31.64	31.31	30.38	32.51	32.68
Na_2O	5.01	5.77	5.23	5.59	5.93	5.17	5.03
	99.56	101.30	99.92	100.20	100.12	100.84	100.27
Structural formula 0=7							
Si	1.999	1.981	2.002	2.000	2.000	2.002	1.990
Al	0.337	0.452	0.401	0.443	0.428	0.364	0.370
Fe	0.254	0.212	0.231	0.225	0.258	0.229	0.265
Mn	0.011	0.000	0.011	0.000	0.008	0.009	0.000
Mg	0.415	0.357	0.373	0.338	0.345	0.403	0.370
Ca	1.593	1.538	1.549	1.523	1.485	1.580	1.605
Na	0.449	0.502	0.464	0.492	0.525	0.455	0.448
$CaNaAlSi_2O_7$ (molec. percent[a])	33.1	44.4	39.9	44.0	42.6	36.2	36.8
$Ca_2MgSi_2O_7$ (molec. percent[a])	40.8	35.0	37.1	33.6	34.3	40.1	36.8
$CaNaFeSi_2O_6$ (molec. percent[a])	11.1	4.9	6.3	4.9	9.7	9.1	7.8
$Ca_2FeSi_2O_7$ (molec. percent[a])	15.0	15.7	16.7	17.5	13.4	14.6	18.6
$Ca_2Al_2SiO_7$ (molec. percent[a])	0	0	0	0	0	0	0
mg (Mg/(Mg+Fe))	0.620	0.627	0.618	0.600	0.572	0.637	0.582
Na/(Na+Ca)	0.220	0.246	0.231	0.244	0.261	0.224	0.218

[a] Deficiencies of Si and excesses of Fe and Ca in some analyses represent <1 ion%

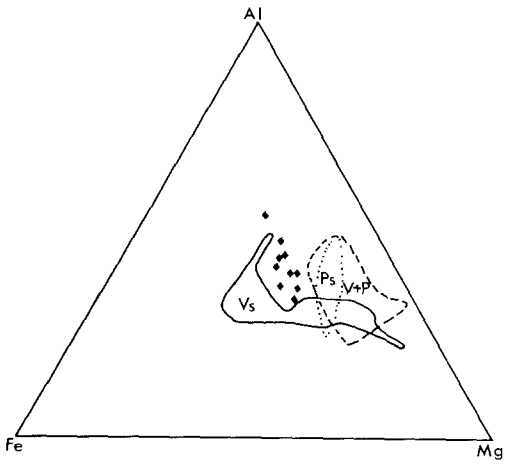

Fig. 2. Fe-Mg-Al (atomic percent) diagram for Oldoinyo Lengai melilites (diamonds). *Vs* and *Ps* are fields of volcanic and plutonic melilites respectively after Sahama (1967); *V+P* is the field for volcanic and plutonic melilites after El Goresy and Yoder (1974). (Note that all the Al is associated with Na (Table 5) and hence is proportional to amount of sodic melilite present)

rich crystals reported by these workers (Fig. 2). Velde and Yoder (1977) have noted that the sodic melilite content of melilites is directly proportional to the normative nepheline content of the host rock or the parent melt. Their data suggest that the Oldoinyo Lengai melilites grow in a melt containing 30–40 wt% nepheline.

An unusual feature of the melilite analyses is the variable content of Mn – in some crystals it is below detection limit, whereas in others it is about 0.25 wt%; it is particularly clear from the paucity of Mn in the middle zone of the step-zoned crystal (Table 5, No. 3) that the Mn content of the melilite is not controlled by the position of the mineral in the crystallisation sequence. The control of the Mn content appears to be very localized and may well result from preferential incorporation of Mn into titanomagnetite or garnet, the latter being included in melilite.

5. Nepheline (Table 6). There are only small compositional differences between nepheline crystals, the largest variations being in Ca, Fe and K; however only Ca shows any systematic relationship to crystal shape (i.e., to crystal growth rate) with the dendritic, most rapidly-grown crystals having approximately twice the Ca content of the euhedral crystals. The analysis of a crystal in a melt inclusion within a hollow apatite crystal (Fig. 6; Table 6, no. 6) is broadly comparable to those of the euhedral, parallel-growth and dendritic nephelines of the groundmass. Compared with zoned nephelines from a loose block of nephelinite found on the lower northern slopes of the volcano (Brown, 1970), the present nephelines are lower in Si but higher in Al, Ca and K (with lower Na/K ratios).

Table 6. Nepheline analyses

	1 Euhedral crystal	2 Euhedral lath	3 Skeleton	4 Parallel-growth	5 Feather dendrite	6 Within melt inclusion in skeletal apatite
SiO_2	42.56	40.58	41.21	42.88	40.78	40.03
Al_2O_3	32.92	32.24	32.02	31.51	32.34	32.76
Fe_2O_3[a]	2.32	2.23	2.52	1.62	1.61	2.32
CaO	0.30	0.32	0.38	0.45	0.61	0.65
K_2O	6.37	8.13	7.29	6.32	6.58	7.77
Na_2O	15.87	15.88	15.45	16.49	16.85	15.97
	100.34	99.38	98.87	99.27	98.77	99.50
Structural formula 0=4						
Si	1.032	1.010	1.024	1.052	1.012	0.995
Al	0.941	0.945	0.938	0.911	0.946	0.960
Fe	0.042	0.042	0.047	0.030	0.030	0.043
Ca	0.008	0.009	0.010	0.012	0.016	0.017
K	0.197	0.258	0.231	0.198	0.208	0.246
Na	0.746	0.766	0.745	0.785	0.811	0.770
Ne wt %	74.4	72.8	72.9	75.9	77.8	73.8
Ks wt %	21.9	27.2	25.1	21.3	22.2	26.2
Qz	3.7	def.[b]	2.0	2.8	def.[b]	def.[b]

[a] All Fe as Fe_2O_3
[b] Deficient in SiO_2

Table 7. Garnet analysis

		Structure O=12		
SiO_2	34.12			
TiO_2	15.29			
Al_2O_3	1.59	Si	2.734	
Fe_2O_3[a]	17.84	Ti	0.936	4.954
MnO	0.10	Al	0.150	
MgO	1.55	Fe^{3+}	1.134	
CaO	30.12	Mn	0.005	
		Mg	0.182	2.873
	100.61	Ca	2.686	

[a] All iron reported as Fe_2O_3 (Poor analysis due to small grain size)

Table 8. Vishnevite analyses

	1 Hopper skeleton	2 Ver-micular crystal		1 Hopper skeleton	2 Ver-micular crystal
SiO_2	35.56	34.86	Structural formula 12 (Si+Al)		
Al_2O_3	29.94	27.94			
Fe_2O_3[a]	1.01	2.20	Si	6.022	6.170
CaO	1.70	1.76	Al	5.978	5.830
Na_2O	21.03	21.55	Fe^{3+}	0.129	0.290
K_2O	1.24	1.16	Ca	0.307	0.333
SO_3[b]	5.19	6.93	Na	6.906	7.394
Cl	1.80	0.99	K	0.269	0.261
			SO_4	0.660	0.920
	97.47	97.39	Cl	0.517	0.298

[a] All Fe reported as Fe_2O_3 [b] All S reported as SO_3

6. Garnet (Table 7. The poor quality of the analysis is believed to result from the small size of the garnets). The garnet is an andradite rich in TiO_2 and may be termed schorlomite. Compared with schorlomite from the ?1966 ash eruption of the volcano (Huggins et al., 1976) the analysed garnet contains higher TiO_2, Al_2O_3 and MgO but lower Fe_2O_3.

7. Vishnevite (Table 8). The widest variations in the vishnevite analyses are in Al, Fe^{3+}, S and Cl. All analyses sum to approximately 97.5 wt% and, if the remaining 2.5% is assumed to be all CO_2, the maximum amount of cancrinite molecule in solid solution with the veshnevite is 40–48 mol %.

8. Residual glass (Table 9). The residual glass compositions vary from point to point, depending on the proximity of crystalline phases. The compositions have low *mg* values ranging from 0.28–0.12. The decrease in *mg* is accompanied by decrease in Ca and SO_3 and by increases in Al, Ti, Mn, Cl and P. These differences are probably attributable to local effects, e.g., extent of zoning of adjacent crystals and amount of local crystallization. The larger content of SO_3 compared to Cl in the vishnevite is believed to be responsible for the contrasting behaviour of S and Cl enrichments in the glasses. The analyses totals lack 4.7–8.5 wt%, and presumably this is predominantly CO_2 and H_2O; for convenience, in calculating norms the shortfall is assumed to be all CO_2. The glass compositions do not approximate to any known peralkaline rocks from Oldoinyo Lengai (Fig. 3 and Dawson, unpublished data) or elsewhere – the combination of high alkalis and low Al makes them unique.

(The CIPW norm is not appropriate for these alkalic undersaturated glasses; rather that for feldspathoidal rocks (Le Bas, 1973) has been adopted. This has been modified in two ways: (i) the exceptionally low Al has necessitated the calculation of potassium silicate (in addition to sodium silicate) and (ii) instead of the

Table 9. Residual glass analyses

	1	2	3		4
			Area 1	Area 2	Partially crystallized melt inclusion in apatite (Fig. 6)
SiO_2	37.90	40.43	39.58	40.35	38.39
Al_2O_3	3.90	5.60	4.74	4.63	3.43
TiO_2	0.69	2.43	1.45	2.00	2.58
Fe_2O_3	3.46	4.58	3.70	4.20	3.99
FeO	8.44	11.77	8.97	10.15	9.65
MnO	0.57	0.61	0.70	0.00	0.90
MgO	2.26	1.34	2.31	2.40	2.42
CaO	13.53	6.97	10.83	12.54	15.43
Na_2O	14.97	13.35	12.97	12.81	13.82
K_2O	4.35	5.35	4.71	4.78	2.81
SO_3	1.49	1.09	1.14	1.25	0.93
Cl	0.25	0.69	0.39	0.27	0.46
P_2O_5	0.00	0.43	0.00	0.33	0.00
	91.55[b]	93.68	91.19	95.35	94.82
mg	0.323	0.168	0.313	0.295	0.309
Wt. percent norm[c]					
orthoclase	–	6.67	6.05	1.10	–
albite	–	18.01	16.59	2.69	–
nepheline	10.79	2.34	1.16	11.56	10.51
sodium silicate	7.12	4.64	2.05	7.61	10.49
potassium silicate	1.35	3.39	1.38	3.82	0.62
halite	0.40	1.10	0.63	0.46	0.75
acmite	9.89	13.40	10.52	11.88	11.55
thenardite	2.63	1.99	1.97	2.25	1.70
akermanite	0.80	–	–	–	2.46
iron-akermanite	2.07	–	–	–	6.69
diopside	10.33	1.52	7.50	10.28	9.09
hedenbergite	26.55	9.18	20.36	27.97	25.54
wollastonite	5.76	–	–	–	1.16
forsterite	0.07	1.82	1.52	0.83	0.28
fayalite	0.30	13.47	5.24	2.72	1.02
sphene	1.33	5.88	3.49	4.85	2.55
perovskite	0.26	–	–	–	2.58
apatite	–	1.00	–	0.66	–
sodium carbonate[d]	11.35	8.69	11.95	6.40	7.10
potassium carbonate[d]	3.63	2.90	3.96	2.05	2.35
calcium carbonate[d]	5.35	4.10	5.64	2.96	3.40

[a] Calculated from Fe^{2+}/Fe^{3+} ratio of groundmass pyroxene (Table 5, no. 5)

[b] Deficiency in totals assumed to be CO_2

[c] Modified (see text) from method of Le Bas, 1973

[d] Allotted in mole ratio 4:1:2 $Na_2O:K_2O:K_2O:CaO$, as in analysis of fresh Oldoinyo Lengai carbonatite lava (Dawson, unpublished data)

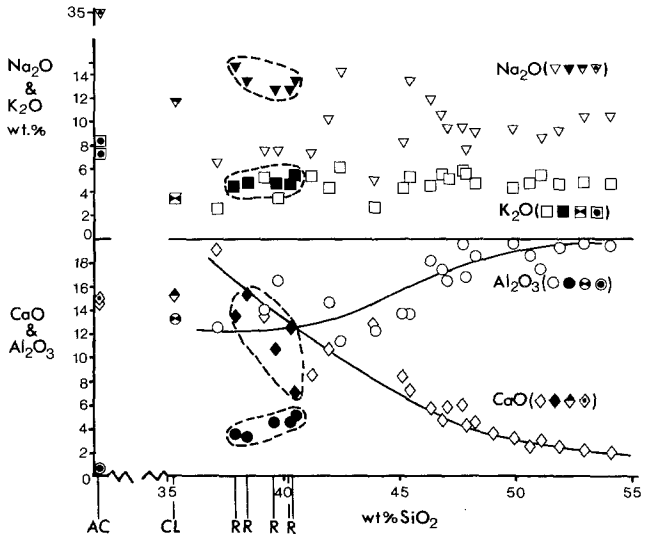

Fig. 3. Plot of SiO_2 *v.* Na_2O, K_2O, CaO and Al_2O_3 (wt percent) in Oldoinyo Lengai phonolite, nephelinite and melanephelinite lavas (open ornament); residual glasses (*R*) (solid ornament) from Table 9; residual glass + crystallites + gas (computed nephelinite liquid-Anal 3, Table 10)-half-filled ornament (*CL*); and alkalic carbonatite lavas (*AC*) – dotted ornament. Lavas from Dawson (1966) and unpublished data. Alkalic carbonatite lavas from Dawson (1962b), recalculated on a water-free basis. Note scale breaks between 1–35% SiO_2 and 15–35% $Na_2O\&K_2O$. (The calculated nephelinite also plots close to extensions of trends for total iron oxide and P_2O_5 (Dawson, 1966, Fig. 2); all other oxides are present in quantities that are too small for significance in this diagram)

(assumed) CO_2 being allocated solely to CaO to form normative calcite, sodium carbonate, potassium carbonate and calcium carbonate have been formed in the mole ratio 4:1:2 $Na_2O:K_2O:CaO$, as in the Oldoinyo Lengai carbonate lavas.)

Crystallisation History

The alkalic pyroxenite nodule represents a crystal-liquid mush comprising the fractional crystallisation products of a silicate magma and quenched interstitial liquid. A possible source is from the floor or walls of a magma chamber as a sample of cumulus crystals and intercumulus liquid. Alternatively, the abundance of pyroxene megacrysts could result from flow differentiation in a dyke or sill, but lacking any textural evidence of flow we assume the cumulate origin. The low jadeite content of the pyroxenes suggests a shallow-level magma chamber.

The earliest phases to crystallize were apatite followed by pyroxene, perovskite and titanomagnetite. Due to their larger crystal sizes and higher densities the latter three minerals settled rapidly and most (if not all) of the megacryst apatite reached the chamber

floor entrapped in pyroxene (e.g., Fig. 1 b). The intercumulus liquid continued to crystallize apatite together with melilite, nepheline and pyroxene. A portion of the partially consolidated alkalic pyroxenite was then rapidly transported to the surface as xenoliths in phonolite magma, and during transport and eruption the residual melt in the xenolith vesiculated and precipitated new crystals of apatite, nepheline, melilite and vishnevite, all of which grew rapidly in skeletal and dendritic fashion.

In the case of cancrinite (the carbonate analogue of vishnevite), the mineral is generally believed to form by reaction of early-crystallizing nepheline with CO_2-rich residual liquids (Saether, 1957). Vishnevite-cancrinite group mineral can also form as an alteration product of sodalite (Thugutt, 1946). In the Oldoinyo Lengai alkali pyroxenite, the vishnevite differs both in crystal size and habit from the nepheline, and does not mantle nepheline. Also, calcite is a very minor phase (<0.1 vol %). The sample is particularly fresh which is inconsistent with an origin of vishnevite by alteration. Textural evidence in the form of multiple crystal shapes indicates that the vishnevite is a primary phase that crystallized from the melt, though we a stress that its presence is probably due to rapid, non-equilibrium fractional crystallization of the parent melt. Under slower cooling conditions and more complete reaction between melt and crystals, vishnevite might not have crystallized.

The unusual residual glass compositions are also the result of the unique fractionation conditions of rapid, non-equilibrium crystallization. Hence, despite the fact that the intercumulus melt had the composition of nephelinite (Table 10, column 3, see later), it is not surprising that the residual glass compositions have no rock counterparts in the world, since the conditions necessary for the formation of the glass are unsuitable for segregation of the glass (melt) into a substantial body.

Intercumulus Melt Composition and Parental Liquid of the Silicate Lavas

We have proposed that the alkalic pyroxenite block is a cumulate with rapidly quenched intercumulus liquid from which some CO_2 and H_2O was lost during vesiculation and eruption. Unfortunately the composition of the parental liquid of the pyroxenite is unknown since the bulk-rock analysis (Table 2) is obviously weighted in favour of the cumulus phases, particularly pyroxene. Even the bulk-rock composition varies from area to area, since the composition as deduced from a direct bulk-rock analysis (Table 2)

Table 10. Compositions of various parts of the thin section for which the modal analysis (Table 1) was obtained (nos. 1–3); calculated from the mode and electron-microprobe analyses of the phases. (Calculated to 100%)

Wt. percent		1 Whole rock	2 Total mega-crysts	3 Ground-mass + vesicles[a]	4 Homa Bay parent magma
SiO_2		41.3	44.7	35.3	43.2
TiO_2		4.3	5.1	1.0	2.5
Al_2O_3		7.0	4.9	13.4	12.8
Fe_2O_3		3.1	3.4	2.7	7.0
FeO		5.5	5.1	5.1	5.1
MnO		0.1	0	0.3	0.3
MgO		9.2	11.1	2.2	5.9
CaO		22.9	24.8	15.1	12.6
Na_2O		3.4	0.9	11.8	5.8
K_2O		0.8	0	3.3	2.8
SO_3		0.4	0	1.6	–
Cl		0.1	0	0.3	–
P_2O_5		1.2	0	5.3	0.7
CO_2		0.7	0	2.6	1.5
mg		0.74	0.79	0.43	0.67
Wt. percent norm[b]					
ne	($Na_3KAl_4Si_4O_{16}$)	9.19	–	31.54	
cg	($NaAlSiO_4$)	5.68	4.26	6.53	
sod. sil.	(Na_2SiO_3)	–	–	1.34	
ac	($NaFeSi_2O_6$)	–	–	7.85	
th	(Na_2SO_4)	0.57	–	2.84	
geh	($Ca_2Al_2SiO_7$)	8.22	9.04	–	
ak	($Ca_2MgSi_2O_7$)	1.09	–	–	
fe-ak	($Ca_2FeSi_2O_7$)	0.30	–	–	
di	($CaMgSi_2O_6$)	40.85	53.76	10.61	
he	($CaFeSi_2O_6$)	16.02	15.86	16.62	
fo	(Mg_2SiO_4)	2.17	2.03	0.42	
fa	(Fe_2SiO_4)	1.12	0.82	0.53	
hem	(Fe_2O_3)	3.04	3.36	–	
sph	($CaTiSiO_5$)	–	7.06	1.57	
pe	($CaTiO_3$)	7.34	3.81	0.68	
ap	($Ca_5(PO_4)_3(OH)$)	2.69	–	12.43	
hl	(NaCl)	0.12	–	0.47	
cc[c]	($CaCO_3$)	0.40	–	1.70	
nc[c]	(Na_2CO_3)	0.95	–	3.60	
kc[c]	(K_2CO_3)	0.28	–	1.10	

[a] Deficiencies in mineral and residual glass analyses totals assumed to be CO_2 only; hence this is the maximum possible CO_2 content. CO_2 volume per cent in vesicles corrected for density, with density of groundmass assumed to be 2.5 g/cc and the density of CO_2 at 1 bar and 1000° C taken as 0.01 g/cc (Vukalovich and Altunin, 1968); amount of CO_2 in vesicles is approx. 0.25 wt%

[b] After Le Bas, 1973

[c] Alloted in the mole ratio 4:1:2 Na_2O:K_2O:CaO, as in analysis of fresh Oldoinyo Lengai carbonatite lava (Dawson, unpublished)

[d] Estimated composition of the parental magma of the Homa Bay, western Kenya, volcanics (Le Bas, 1977, Table 24.1)

differs from a computed mode/mineral-composition analysis on one thin section (Table 10, No. 1). Nonetheless, it is apparent from the mineral assemblage and the phase compositions that the parental liquid was silica-undersaturated, and extremely calcic (to precipitate pyroxene, perovskite and apatite, in addition to leaving up to 15% CaO in the residual glasses). It was also rich in total iron, alkalis, phosphorus and volatiles.

Since the megacrysts form a rather open cellular texture, the alkalic pyroxenite crystal-liquid mush probably maintained diffusional contact with the parental liquid while in the magma chamber. Hence, the quenched intercumulus liquid will approximate the composition of the parental liquid. (In reality, the quenched liquid is probably slightly depleted in megacryst components compared to the parental liquid owing to growth of megacrysts within the cumulate). The composition of the intercumulus liquid has been computed by combining modal and groundmass phase–composition data (Table 10, no. 3). Despite the large errors to be expected in this estimate, the melt is clearly of nephelinitic composition, specifically of the olivine-poor variety of nephelinites recognised by Le Bas (1977). The large normative nepheline content of the liquid compares well with that predicted from the sodic melilite content of the melilite (see earlier).

Bearing in mind the likely large errors in the estimate, in a Harker diagram (Fig. 3) the nephelinite plots close to extensions of the trend lines for the phonolite-melanephelinite sequence at Oldoinyo Lengai, suggesting that it might be a suitable parental liquid for the sequence. We are currently investigating the modal relations and phenocryst compositions of the silicate lavas, in order to better understand the fractional crystallization and other processes operating in the magma chamber forming the plutonic complex below Oldoinyo Lengai, and to test the suitability of the computed nephelinite as a parental liquid to the suite. The composition is much less mafic than that of the nephelinite computed by Le Bas to be parental to the western Kenya nephelinite-carbonatite province (Table 10).

Relevance of Alkalic Pyroxenite Paragenesis to Formation of the Carbonatite Lavas

The most intriguing problem surrounding petrogenesis of the Oldoinyo Lengai magma types is the nature of the genetic relation between the older silicate and the younger alkali carbonate lavas. The latter have been suggested to be (a) the residuum following extreme fractional crystallization of a silicate magma (e.g., Heinrich, 1966) and (b) the product of liquid immiscibility of a carbonated silicate melt (e.g., Cooper et al., 1975; Le Bas, 1977). Other suggestions that the carbonatite is mobilised trona (Milton, 1968) or that it is a primary magma which desilicated and remobilised the crust to form the silicate lavas (Dawson, 1962a) are discredited by Sr isotope studies (Bell et al., 1973). (We also shall ignore the primary carbonatite magma hypothesis of Koster van Groos (1975a) since it apparently applies to carbonatites much poorer in alkalis and richer in Fe and Mg than the Oldoinyo Lengai natrocarbonatite.)

(a) Fractional Crystallization

The principal chemical features of the alkali carbonatite magma [nil Al_2O_3 and SiO_2 and of higher Na_2O but similar CaO content to the computed parental nephelinite liquid (Fig. 3)] are impossible to achieve by fractionation from the liquid of the minerals known to have been present in the magma chamber (i.e., phenocrysts in the silicate lavas – alkali feldspar, nepheline, melilite, wollastonite, aegerine augite, sodalite, titanomagnetite and perovskite – and crystals in the alkalic pyroxenite nodule). Nor does fractionation of aluminous low-Ca pyroxene, which might crystallize under high P_{CO_2} (Eggler, 1974), help, since the potential orthopyroxene in the nephelinite is a mere 10–15 wt%. This evidence discrediting a fractional crystallization origin for the carbonatite is supported by the large silica gap between silicate and carbonate magmas (Fig. 3), by experiments on Sr fractionation (Koster van Groos, 1975b), and by the reasonably constant Na/K and K/Rb ratios of the silicate and carbonate rock types (Dawson, 1966).

(b) Liquid Immiscibility

The case for liquid immiscibility between carbonate and silicate magmas has been based on experimental studies, predominantly in simple model systems but also, recently, in haplomagmas (Koster van Groos, 1975a). Koster van Groos and Wyllie (1966) observed liquid miscibility between sodium carbonate and albite at 1 atm but confirmed the presence of immiscibility at 33 bars, thus giving direct evidence of pressure-dependent immiscibility in a simple silicate-carbonate system; it was suggested that this might be a mechanism whereby highly reactive carbonate liquids, such as those at Oldoinyo Lengai, could erupt without incorporation of silicate material. There are at present no experimental data on the solubility of CO_2 in

melts comparable to the interstitial liquid in the alkalic pyroxenite nodule, though our data (admittedly dependent on the accuracy of point counting of one thin section) suggests 2–3 wt% CO_2 at low pressure. The low SiO_2 and Al_2O_3 but high Na_2O content of the computed liquid (Table 10) imply a very depolymerized melt which would be unlikely to yield a second, even less polymerized, carbonate melt by low-pressure immiscibility, no matter how much CO_2 is dissolved in it. This liquid is also very rich in CaO and, significantly, Watkinson and Wyllie (1971) did not observe liquid immiscibility in lime-rich synthetic systems; the absence of immiscible carbonate in the alkalic pyroxenite nodule appears to confirm this. In fact, all factors, except P_2O_5, appear to be unfavourable for immiscibility between nephelinite and carbonate liquids at low pressures.

A more attractive silicate magma for development of immiscibility is the phonolite; its higher SiO_2 and Al_2O_3 contents compared to the nephelinite favour polymerization and splitting into two melts. Furthermore, it has a much lower CaO content than the nephelinite. In support of a phonolite-carbonatite connection, Freestone (1978) has noted that the K/Rb ratios of the phonolites and carbonatites are more similar than those of the nephelinite and carbonatite. In addition, Koster van Groos and Wyllie (1973) showed that immiscible carbonate liquid is likely to be richer in CaO than the parent silicate melt; this condition would be fulfilled by phonolite but not by nephelinite (Fig. 3).

We therefore support a liquid immiscibility connection between the alkali carbonatite and silicate lavas. While phonolitic magma appears to be a more attractive candidate for liquid splitting, the possibility of carbonated nephelinite splitting into two melts at high pressure cannot be dismissed. Experimental petrology studies of silicate magma types are needed to test this. In addition, information is needed on the relative amounts of CO_2 and H_2O in the Oldoinyo Lengai silicate magma types, since CO_2 enhances polymerization of silicate liquids whereas H_2O reduces it (e.g., Kushiro, 1975). The ratio between the two components could be critical in determining the depth at which immiscibility is occurring at Oldoinyo Lengai.

Acknowledgements. We thank I an Freestone for discussion, Mike Henderson for reviewing an early draft of the m.s., and also the reviewer for the journal for his useful comments. The bulk of the study was conducted while the first author was a postdoctoral research fellow in the Department of Geology, University of Manchester; he is grateful to NERC for financial support in a grant to Professor W.S. MacKenzie. We thank J.R. Baldwin and R. Fuge for analyses of the bulk rock, and S. Fell and J. Allen for secretarial and technical assistance.

References

Anderson, A.T.: Oxidation of the La Blache Lake titaniferous magnetite deposit, Quebec. J. Geol. **76**, 528–552 (1968)

Bell, K., Dawson, J.B., Farquhar, R.M.: Strontium isotope studies of alkalic rocks: the active carbonatite volcano Oldoinyo Lengai, Tanzania. Geol. Soc. Am. Bull. **84**, 1019–1030 (1973)

Brown, F.H.: Zoning in some volcanic nephelines. Am. Mineralogist **55**, 1670–1680 (1970)

Cooper, A.F., Gittins, G., Tuttle, O.F.: The system Na_2CO_3-K_2CO_3-$CaCO_3$ at 1 kilobar and its significance in carbonatite petrogenesis. Am. J. Sci. **275**, 534–560 (1975)

Dawson, J.B.: The geology of Oldoinyo Lengai. Bull. Volcanol. **24**, 349–387 (1962a)

Dawson, J.B.: Sodium carbonate lavas from Oldoinyo Lengai, Tanganyika. Nature **195**, 1065–1066 (1962b)

Dawson, J.B.: Oldoinyo Lengai: an active volcano with sodium carbonate lava flows. In: Carbonatites (O.F. Tuttle and J. Gittins, eds.), pp. 155–168. New York: Wiley

Dawson, J.B., Bowden, P., Clarke, C.: Volcanic activity of Oldoinyo Lengai, 1966. Geol. Rundschau **57**, 865–879 (1968)

Dawson, J.B., Powell, D.G.: The Natron-Engaruka explosion crater area, northern Tanzania. Bull. Volcanol. **33**, 791–817 (1969)

Deer, W.A., Howie, R.A., Zussman, J.: Rock-Forming Minerals. Vol. 5. (Longmans) (1962)

Donaldson, C.H.: An experimental investigation of olivine morphology. Contrib. Mineral. Petrol. **57**, 187–213 (1976)

Eggler, D.H.: Effect of CO_2 on the melting of peridotites. Carnegie Inst. Washington Yearbook **73**, 215–224 (1974)

El Goresy, A., Yoder, H.S.: Natural and synthetic melilite compositions Ann. Rpt. Dir. Geophys. Lab. **73**, 359–371 (1974)

Freestone, I.C.: Some aspects of liquid immiscibility. Unpubl. Ph.D. thesis, Univ. of Leeds (1978)

Heiken, G.: An Atlas of Volcanic Ash. Smithsonian Contribs. to Earth Sci. **12** (1974)

Heinrich, E.W.: The Geology of Carbonatites. Chicago: Rand McNally and Co. 1966

Huggins, F.E., Virgo, D., Huckenholz, H.G.: The crystal chemistry of melanites and schorlomites. Ann. Rpt. Dir. Geophys. Lab. **75**, 705–711 (1976)

Hutton, C.O.: The igneous rocks of the Brocken range – Ngahayse area, eastern Wellington. Trans. Roy. Soc. New Zealand **72**, 353–363 (1943)

Koster van Groos, A.F.: The effect of high CO_2 pressures on alkalic rocks and its bearing on the formation of alkalic ultrabasic rocks and the associated carbonatites. Am. J. Sci. **275**, 163–185 (1975a)

Koster van Groos, A.F.: The distribution of strontium between coexisting silicate and carbonate liquids at elevated pressures and temperatures. Geochim. Cosmochim. Acta **39**, 27–34 (1975b)

Koster van Groos, A.F., Wyllie, P.J.: Liquid immiscibility in the join $NaAlSi_3O_8$-$CaAl_2Si_2O_8$-Na_2CO_3-H_2O. Am. J. Sci. **273**, 465–487 (1973)

Kushiro, I.: Clinopyroxene solid solutions. Part 1. The $CaAl_2SiO_6$ component. Japanese J. Geol. Geog. **33**, 213–220 (1962)

Kushiro, I.: On the nature of silicate melt and its significance in magma genesis: regularities in the shift of the liquidus boundaries involving olivine, pyroxene, and silica minerals. Am. J. Sci. **275**, 411–431 (1975)

Le Bas, M.J.: A norm for feldspathoidal and melilite rocks. J. Geol. **81**, 89–96 (1973)

Le Bas, M.J.: Carbonatite-Nephelinite Volcanism. London: Wiley 1977

Saether, E.: The alkaline rock province of the Fen area in southern

Norway. Det. Kgl. Norske Videnskabers Selskabs Skrifter **1**, 1–8 (1957)

Sahama, Th.G.: Iron content of melilite. Compt. Rend. Soc. Geol. Finlande **39**, 17–28 (1967)

Sahama, Th.G.: Composition of clinopyroxene and melilite in the Nyiragongo rocks. Ann. Rpt. Dir. Geophys. Lab **75**, 585–593 (1976)

Thugutt, St.J.: Sur la sodalite et ses dérivés. Anh. Min. Soc. Sci. Lett. Varsovie **16**, p. 14 (1946) (Min. Abst. 10–293)

Velde, D., Yoder, H.S.: Melilite and melilite-bearing igneous rocks. Carnegie Inst. Washington Yearbook **76**, 478–485 (1977)

Virgo, D., Mysen, B.O.: Influence of structural changes in $NaAl_{1-x}Fe_xSi_2O_6$ melts on Fe^{3+}-ΣFe ratios. Carnegie Inst. Washington Yearbook **76**, 400–407 (1977)

Vukalovich, M.P., Altunin, V.V.: Thermophysical Properties of Carbon Dioxide. London: Collet's 1968

Watkinson, D.H., Wyllie, P.J.: Experimental study of the composition join $NaAlSiO_4$-$CaCO_3$-H_2O and the genesis of alkalic rock complexes. J. Petrol. **12**, 357–378 (1971)

Wilkinson, J.F.G.: The clinopyroxenes of a differentiated teschenite sill near Gunnedah, New South Wales. Geol. Mag. **94**, 123–134 (1957)

Wyllie, P.J., Cox, K.G., Biggar, G.M.: The habit of apatite in synthetic melts and natural rock systems. J. Petrol. **3**, 238–243 (1962)

Received March 30, 1978 / Accepted June 8, 1978